Transient and sustained visuomotor selection during working-memory guided behavior.

Edward F. Ester[1,2], Rachel Weese[1]

[1]Department of Psychology, University of Nevada, Reno
[2]Integrative Neuroscience Program, University of Nevada, Reno

Support: NSF 2050833 (E.F.E.), Nevada Undergraduate Research Award (R.W.)

Contributions: E.F.E. and R.W. conceived and designed the experiment. R.W. collected data, E.F.E. and R.W. analyzed data. E.F.E. and R.W. wrote the manuscript.

Data and Analytic Software: forthcoming!

Abstract

Working memory enables flexible behavior by enabling the storage of sensory information alongside possible actions. Here, we show that access to the sensory and motor contents of working memory are mediated by different selection mechanisms with different time courses. Sensory selection is transient begins and ends prior to the initiation of an overt behavior. Conversely, motor selection begins in parallel with visual selection and persists throughout action planning and execution.

A fundamental purpose of any memory system is to inform future decisions and actions. This is particularly important in the case of working memory (WM), a duration- and capacity-limited system that forms a temporal bridge between fleeting sensory phenomena and possible actions (1). Recent theoretical conceptualizations of WM have begun to emphasize the action-oriented nature of this system (e.g., 2-5), and recent empirical findings suggest that behavioral (6-7), circuit-level (8-10), and systems-level (11-20) mechanisms of WM storage and action planning are tightly interwoven.

Many everyday behaviors require that WM-guided actions be timed to a future event or executed in a specific sequence (e.g., making your favorite cup of coffee involves performing a series of actions in a specific order and only when certain external conditions – e.g., the water in the kettle has begun to boil – have been met). Once a future goal state becomes obvious, what happens to the mnemonic representations of visual and motor information needed to reach it? One possibility is that visuomotor representations are selected and prioritized until a prospective action is executed or completed, enabling precise and continuous memory-guided control of behavior. Alternately, visuomotor representations might be selected and transformed from retrospective stimulus- and rule-based representations into prospective action-based representations (e.g., 6, 10, 19-20).

To evaluate these alternatives, we recorded EEG while 31 human volunteers performed a retrospectively cued orientation memory task (Fig 1a). Participants remembered the orientations of two gratings over a blank delay. 1.5 sec after encoding, a 100% valid color cue indicated which of the two gratings would be probed for report at the end of the trial and which hand should be used for memory recall (i.e., left or right; response hand/cue color mappings were counterbalanced across participants). A response display containing a vertically oriented grating was presented 1.0 seconds later; participants adjusted the orientation of this probe to match the orientation of the grating held in memory using the cued response hand. Participants performed this task well, recalling the orientation of the probed grating with an average (±1 S.E.M.) absolute error of 13.6° ± 0.75° and responded with the correct hand on 93.8% ± 0.89% of trials.

To examine how visual and motor WM representations contribute to future behaviors, we identified neural signals associated with the selection of visual and motor information in EEG data by independently manipulating the physical location of the cue-matching stimulus (i.e., left vs. right visual field) and the cued response hand (i.e., left vs. right) across trials. This allowed us to track trial-averaged signals associated with selecting visual and motor WM representations independent of any volume conduction or signal mixing. While this approach is familiar from earlier work (e.g., 17), our task additionally allowed us to probe the dynamics of visuomotor selection during development of a *planned* action: upon presentation of retrocue display participants were free to select task-relevant visuomotor representations stored in WM but could not execute a response until one second later.

We considered three models describing how visual and motor WM representations might contribute to future behaviors (Fig 1a-c). In the first model (Fig 1a), task-relevant visual and motor WM representations are selected immediately after cue onset, and these representations remain prioritized until a final response is made. In the second model (Fig 1b), task-relevant visuomotor selection is delayed until action is imminent. In the third model (Fig 1c), task-relevant visual and motor WM

representations are selected immediately after cue onset. However, once selected, visual WM representations are used to fine-tune prospective actions and/or discarded, yielding a pattern of transient visual selection and persistent motor selection.

We tested these models by tracking neural signals associated with the selection of visual and motor information stored in memory in near-real-time (tens of milliseconds). We first identified EEG signals that co-varied with the physical location of the retrospectively cued stimulus (i.e., left vs. right visual hemifield; Fig 2a) and EEG signals that co-varied with the retrospectively cued response hand (i.e., left vs. right; Fig 2b). Because stimulus location and response hand were independently manipulated over trials (i.e., a stimulus requiring a right-hand response was equally likely to appear in the left vs. right visual field) we were able to characterize the selection of both attributes in trial-averaged EEG data independently of one another. Thus, we attributed patterns of neural activity that covaried with stimulus location to the selection of visual information stored in WM and patterns of neural activity that covaried with response hand to the selection of motor information stored in WM.

Visual selection was associated with a robust but transient decrease in 8-13 Hz alpha power over electrode sites contralateral to the location of the cued stimulus (Fig 2a). This modulation was strongest over occipitoparietal electrode sites (Fig 2a; inset), consistent with prior reports linking changes in lateralized alpha power to shifts of attention in perception and WM (17; 21-22). Conversely, motor selection was associated with a robust and sustained decrease in 8-13 Hz mu-alpha power and 15-30 Hz beta power over electrode sites contralateral to the location of the cued response hand (Fig 2b). This modulation was strongest over frontocentral electrode sites (Fig 2b; inset), consistent with prior reports linking changes in lateralized alpha power to shifts of attention in perception and WM (17; 23). Direct comparisons of EEG signals associated with visual and motor selection revealed transient and sustained visual and motor selection lasting approximately 300-900 ms and 300-3000 ms after retrocue onset, consistent with the hybrid selection model sketched in Fig 1d.

In a complementary analysis, we decoded the location of the retrospectively cued stimulus (i.e., left vs. right visual hemifield) and the retrospectively cued response hand (i.e., left vs right) from broadband (1-50 Hz) EEG responses measured over occipitoparietal and frontocentral electrode clusters where spectral signals associated with visual and motor selection were largest (occipitoparietal 10-20 electrode sites O1/2, PO3/4, PO7/8 and frontocentral 10-20 electrode sites C1/2 and C3/4; Fig 3). This allowed us to probe task-relevant information in evoked (as compared to induced) EEG activity with an even greater temporal resolution (i.e., absent all but the most liberal spectral filters needed to remove low-frequency drifts and line noise from the EEG signal). We also attempted to decode the orientations of the cued and uncued gratings but were unable to do so except during the probe period where a physical orientation was present on the screen (Fig S1).

A comparison of stimulus location and response hand decoding performance over occipitoparietal electrode sites (Fig 3a) revealed transient above-chance decoding of stimulus location during the delay separating the retrocue and probe displays. However, these effects were dwarfed by robust decoding of response hand over the cue-to-probe interval and during the response period. An identical analysis of stimulus location and response hand decoding performance over frontocentral electrode sites

(Fig 3b) revealed a complementary pattern, with stimulus location decoding performance reaching above chance levels for a brief interval only during the cue-to-probe delay and response hand decoding performance reaching above-chance levels during both the cue-to-probe delay and during the response period. Thus, motor signals dominate memory signals over occipitoparietal and frontocentral electrode sites when planning or executing a memory-guided behavior.

Although several recent studies have examined circuit-, network-, and brain-level interactions between WM and motor planning during imminent action (17-20), to our knowledge no study has examined how visuomotor representations stored in WM used to plan and implement future actions. Leveraging the high temporal resolution of human EEG recordings, we show that when planning a memory-guided behavior the brain initially selects task-relevant visual and motor information stored in WM, but the selection of visual WM content ends well before an overt action is produced.

Since stimulus location was an incidental feature of our task, one could argue that observations of transient visual selection based on stimulus location (e.g., Fig 2c, Fig 3) are also incidental. However, several lines of evidence indicate that position information is automatically and inextricably bound to other visual features stored in WM: Position-specific signals can be decoded from scalp EEG activity during WM tasks where stimulus location is task-irrelevant (e.g., 24) or from population spiking activity in prefrontal, parietal, and visual cortex following a cue that renders stimulus location task-irrelevant (e.g., 10). Other studies have documented gaze biases towards task-relevant stimuli during WM tasks where stimulus location is task-irrelevant (e.g., 18-19, 25).

Transient selection of visual information in WM might reflect a strategic removal of previously relevant content from WM that frees mnemonic resources for processing other sensorimotor representations or motor signals (e.g., 26). Alternately, transient selection of visual information in WM could reflect the operation of mechanisms that transform retrospective, stimulus-oriented memory representations into prospective, action-oriented representations. This explanation dovetails with recent findings from cellular and systems neuroscience demonstrating that population-level representations of WM content are mapped into new subspaces following changes in priority or behavioral relevance (e.g., “rotational remapping”; 10; 27-28). These alternatives are non-exclusive and await further investigation. Nevertheless, our findings shed new light on processes mediating memory-guided behaviors by demonstrating that access to the sensory and motor contents of working memory are mediated by different selection mechanisms with fundamentally different time courses.

References

1. D'Esposito M, Postle BR. The cognitive neuroscience of working memory. Annual Review of Psychology, 66:115-142 (2015)

2. Buschman TJ. Balancing flexibility and interference in working memory. Annual Review of Vision Science, 7:367-388 (2021)

3. van Ede F., Nobre AC. Turning attention inside out: How working memory serves behavior. Annual Review of Psychology (2022)

4. Heuer A, Ohl S, Rolfs M. Memory for action: A functional view of selection in working memory. Visual Cognition 28 (2020)

5. Olivers CNL, Roelfsema PR. Attention for action in visual working memory. Cortex 131:179-194 (2020)

6. Gonzalez-Garcia C, Formica S, Liefooghe B, Brass M. Attentional prioritization reconfigures novel instructions into action-oriented task sets. Cognition 194:104059 (2020)

7. Ohl S, Rolfs M. Bold moves: Inevitable saccadic selection in visual short-term memory. Journal of Vision 20(2):11 (2020)

8. Tang C, Herikstad R, Parthasarathy A, Libedinsky C, Yen S-C. Minimally dependent activity subspaces for working memory and motor preparation in the lateral prefrontal cortex. eLife:9e58154 (2020)

9. Pho GN, Goard MJ, Woodson J, Crawford B, Sur M. Task-dependent representations of stimulus and choice in mouse parietal cortex. Nature Communications, 9:1-16 (2018)

10. Panichello M, Buschman T. Shared mechanisms underlie the control of working memory and attention. Nature 592:601-605 (2021)

11. Chatham CH, Frank MJ, Badre D. Corticostriatal output gating during selection from working memory. Neuron 81:930-942 (2014)

12. Minxha J, Adolphs R, Fusi S, Mamelak AN, Rutishauser U. Flexible recruitment of memory-based choice-representations by the human medial frontal cortex. Science, 368:eaba3313 (2020)

13. Galero-Salas Y, Han S, Sych Y, Voigt FF, Laurenczy B, Gilad A, Helmchen F. Sensory and behavioral components of neocortical signal flow in discrimination tasks with short-term memory. Neuron, 109:135-148 (2021)

14. Rac-Lubashevsky R, Frank MJ. Analogous computations in working memory input, output and motor gating: Electrophysiological and computational modeling evidence. PLoS Computational Biology 17:e1008971 (2021)

15. Henderson MM, Rademaker RL, Serences JT. Flexible utilization of spatial- and motor-based codes for the storage of visuo-spatial information. eLife, 11:e75688 (2022)

16. Ariani G, Pruszynski JA, Diedrichsen J (2022) Motor planning brings human primary somatosensory cortex into action-specific prepatory states. eLife 11:e69517 (2022)

17. van Ede F, Chekroud SR, Stokes M, Nobre AC. Concurrent visual and motor selection during visual working memory guided behavior. Nature Neuroscience, 22:477-483 (2019)

18. van Ede F, Deden J, Nobre AC. Looking ahead in working memory to guide sequential behavior. Current Biology 31:R779-R780 (2021)

19. van Ede F, Deden J, Nobre AC. Planning the potential future during multi-item visual working memory. bioRxiv (2021)

20. Boettcher SEP, Gresch D, Nobre AC, van Ede F. Output planning at the input stage in visual working memory. Science Advances 7:eabe8212 (2021)

21. van Ede F. Mnemonic and attentional roles for states of attenuated alpha oscillations in perceptual working memory: a review. European Journal of Neuroscience, 48:2509-2515 (2018)

22. Klimesch W. Alpha-band oscillations, attention, and controlled access to stored information. Trends in Cognitive Sciences, 16:606-617 (2012)

23. Jenkinson N, Brown P. New insights into the relationship between dopamine, beta oscillations, and motor function. Trends in Neurosciences, 34:611-618 (2018).

24. Foster JJ, Bsales EM, Jaffe RJ, Awh E. Alpha-band activity reveals spontaneous representations of spatial position in visual working memory. Current Biology, 27:3216-3223 (2017)

25. van Ede F, Chekroud SR, Nobre AC. Human gaze tracks attentional focusing in memorized visual face. Nature Human Behavior 3:462-470 (2019)

26. Souza AS, Rerko L, Oberauer K. Unloading and reloading working memory: Attending to one item frees capacity. Journal of Experimental Psychology: Human Perception & Performance 40:1237-1256. (2014)

27. Libby A, Buschman TJ. Rotational dynamics reduce interference between sensory and memory representations. Nature Neuroscience 24:715-726 (2021)

28. Wan Q, Menendez JA, Postle BR. Priority-based transformations of stimulus representation in visual working memory. bioRxiv. https://doi.org/10.1101/2021.05.13.443973

Supporting Online Methods

Research Participants. 32 human volunteers (both sexes) from the University of Nevada, Reno community completed a single 2.5-hour testing session in exchange for monetary remuneration ($15/h). All volunteers self-reported normal or corrected-to-normal visual acuity and gave both written and oral informed consent before enrolling in the study. Data from one participant who completed the study were excluded from final analyses due to chance-level task performance (i.e., the participant used the correct response hand on only 52% of trials); thus, the findings reported here reflect the remaining 31 participants.

Testing Environment. Participants were seated in a dimly lit room for the duration of testing. Visual displays were generated in MATLAB and rendered on a 27-inch LCD monitor (1920 x 1080 resolution) cycling at 240 Hz using Psychophysics Toolbox software extensions (29). Participants were seated approximately 80 cm from the display (head position was not constrained). Participants responded via buttons on a standard US computer keyboard.

Visuomotor Recall Task. A task schematic is shown in Figure 1A. Each trial began with a 500 ms sample display containing two colored gratings (radius 4.5° visual angle [DVA] from a viewing distance of 80 cm; 1.0 cycles/°) presented 7.0 DVA to the left and right of a central fixation point. The sample display was followed by a 1500 ms blank display and a 1000 ms retrospective cue display. The color of the retrospective cue instructed participants which grating would be probed at the end of the trial (i.e., blue or red) and which hand should be used to make a behavioral response (left or right). Cue-response mappings (i.e., red cue/left vs. right hand) were counterbalanced across participants. Each trial ended with a 2000 ms probe display containing a vertically oriented grating; participants recalled the orientation of the cued grating by adjusting the probe grating to match the corresponding sample grating using the cue-specific response hand. If participants were satisfied with their response before the end of the 2000 ms, they were instructed to refrain from pressing any other buttons. Participants completed 3 (N = 1), 7 (N = 2), or 8 (N = 28) blocks of 60 trials. Due to a coding error, we were unable to estimate response times (i.e., elapsed time between the onset of the probe display and the participant's initial button press) for any of the 31 participants.

EEG Acquisition & Preprocessing. Continuous EEG was recorded from 63 scalp electrodes using a BrainProducts actiCHamp system using a left mastoid reference (10-20 electrode site TP9). Data were digitized at 1 kHz and later re-referenced to the algebraic mean of the left and right mastoids (using 10-20 site TP10 as the right mastoid reference). The following preprocessing steps were applied, in order: (1) resampling from 1 kHz to 500 Hz; (2) bandpass filtering from 1 to 50 Hz (zero-phase forward- and reverse- finite impulse response filters as implemented by EEGLAB software extensions; 30); (3) identification, removal, and reconstruction of noisy epochs via artifact subspace reconstruction (implemented via EEGLAB; 31-32), (4) epoching from -1.0 to +5.0 sec relative to the start of each trial, and (5) application of a surface Laplacian to remove low spatial frequency components from the signal (33).

Spectral Analyses. Spectral analyses focused occipitoparietal and frontocentral 10-20 electrode site pairs O1/2, PO3/4, PO7/8, C1/C2, and C3/C4; analyses were restricted to a period spanning -500 to +2500 ms before and after retrocue onset. We extracted broadband spectral power from each electrode on each trial using a short-time Fourier transform (STFT) with a frequency range from 1-40 Hz (in 0.25 Hz steps) using a 200 ms sliding window and 2 ms step size. Power was computed by squaring the absolute value of the complex Fourier coefficients within each STFT window.

To quantify changes in lateralized activity during visual selection, we sorted power estimates at each occipitoparietal electrode site by the location of the retrospectively cued stimulus, i.e., contralateral vs. ipsilateral hemifield, and expressed this difference as a normalized percentage:

$$L_i = 100 \times \frac{(c_i - s_i)}{(c_i + s_i)}$$

where c_i and s_i are the trial-averaged responses of electrode *i* when the retrospectively cued grating appeared in the contralateral or ipsilateral visual field, respectively. Lateralization estimates were pooled across occipitoparietal electrode sites, yielding a single time-frequency matrix of power estimates per participant. These matrices were averaged across participants to produce the data shown in Fig 2A.

An identical approach was used to quantify changes in lateralized activity during motor selection, with the exceptions that (a) analyses focused exclusively frontocentral electrode sites, and (b) trial-wise power estimates were sorted by the retrospectively cued response hand rather than stimulus location. This analysis was used to generate the data shown in Fig 2B.

To generate the topographical maps of alpha- and beta-band lateralization shown in Figs 2A and 2B, we repeated this analysis for every scalp electrode and averaged power estimates over 8-13 Hz (“alpha-band” activity) and 15-30 Hz (“beta-band” activity) over a period from 500-1000 Hz. These frequency bands were chosen a priori based on commonly reported values in the literature (e.g., 23-25); this specific temporal window was chosen a priori based on prior reports suggesting that it takes human observers ~300-500 ms to process and respond to a retrospective memory cue (e.g., 26).

An analogous procedure was used to measure frontocentral beta-power lateralization, with the exceptions that (a) analyses focused on frontocentral electrode sites and (b) trial-wise recordings were sorted as contralateral or ipsilateral relative to the retrospectively cued response hand.

To visualize changes in occipitoparietal alpha power, frontocentral mu-alpha power, and frontocentral beta power (e.g, Fig 2C), we extracted and averaged lateralization

estimates from 8-13 Hz over electrode sites O1/2, PO3/4, and PO7/8, lateralization estimates from 8-13 Hz over electrode sites C1/2, C3/4, and lateralization estimates from 15-30 Hz over electrode sites C1/2, C3/4. Statistical analyses of lateralization were performed using nonparametric sign permutation tests with temporal cluster-based correction (see *Statistical Analyses*, below).

Stimulus Location and Response Hand Decoding. Decoding analyses (Fig 3; Fig S2) were applied to broadband (1-50 Hz) signals measured at occipitopartietal electrode sites O1/2, PO3/4, PO7/8 and frontocentral electrode sites C1/2, C3/4. Decoding performance was computed separately for each time sample using 10-fold cross-validation. During each cross-validation fold, we designated 90% of available trials as a training data set and the remaining 10% of trials as a test data set, taking care to ensure that the training data set contained an equal number of observations for each possible outcome (e.g., for stimulus location decoding, we ensured that the training data set contained an equal number of left- and right visual field trials; likewise, for response hand decoding we ensured that the training data set contained an equal number of left- and right-hand trials). Decoding performance was computed by fitting a multivariate normal density to observations associated with each class in the training data set (using a pooled diagonal covariance matrix estimate), then assigning observations in the test data set to groups based on likelihood ratios. Qualitatively similar findings were obtained using other decoding approaches (e.g., using multivariate distance as in 34-35; Fig S2).

Decoding performance was quantified by computing the proportion of test trials where the classifier predicted the correct stimulus location or response hand. Performance estimates were averaged across cross-validation folds, yielding a single stimulus location and response hand decoding time series per participant and electrode cluster (i.e., occipitoparietal vs. frontocentral). Since stimulus location and response hand were binary variables, we evaluated decoding performance against a chance level of 50%.

Statistical Comparisons. All statistical comparisons reported here were based on nonparametric sign permutation tests (36). Specifically, each test we performed assumes a null statistic of 0 (i.e., no difference in alpha- or beta-band lateralization, or no difference in observed vs. chance decoding performance). We therefore generated null distributions of the differences between dependent variables (e.g., alpha- and beta-band lateralization, or location vs. response hand decoding) by randomly relabeling each participant's data with 50% probability and averaging the data across participants. This step was repeated 10,000 times, yielding a 10,000-element null distribution for each time point. Finally, we implemented a cluster-based permutation test with cluster-forming and cluster-size thresholds of $p < 0.05$ to evaluate differences with respect to this null distribution while correcting for multiple comparisons across time.

Online References

29. Kleiner M, Brainard D, Pelli D. What's new in Psychtoolbox-3? iPerception 36 (2007)

30. Delorme A, Makeig S. EEGLAB: An open-source toolbox for analysis of single-trial EEG dynamics including independent component analysis. Journal of Neuroscience Methods 134:9-21 (2004)

31. Chang C-Y, Hsu S-H, Pion-Tonachini L, Jung T-P. Evaluation of Artifact Subspace Reconstruction for automatic artifact components removal in multi-channel EEG recordings. IEEE Transactions on Biomedical Engineering, 67(4) (2019)

32. Blum S, Jacobsen NSJ, Bleichner MG, Debener S. A Reimannian modification of Artifact Subspace Reconstruction for EEG artifact handling. Frontiers in Human Neuroscience 141 (2019)

33. Perrin F, Pernier J, Bertrand O, Echallier JF. Spherical splines for scalp potential and current density mapping. Electroencephalography and Clinical Neurophysiology, 72:184-187 (1989)

34. Wolff MJ, Jochim J, Akyurek EG, Stokes MG. Dynamic hidden states underlying working-memory-guided behavior. Nature Neuroscience 20:864-871 (2017)

35. Wolff MJ, Kandemir G, Stokes MG, Akyurek EG. Unimodal and bimodal access to sensory working memories by auditory and visual impulses. Journal of Neuroscience, 40:671-681 (2020)

36. Maris E, Oostenveld R. Nonparametric statistical testing of EEG and MEG data. Journal of Neuroscience Methods, 164:177-190 (2007)

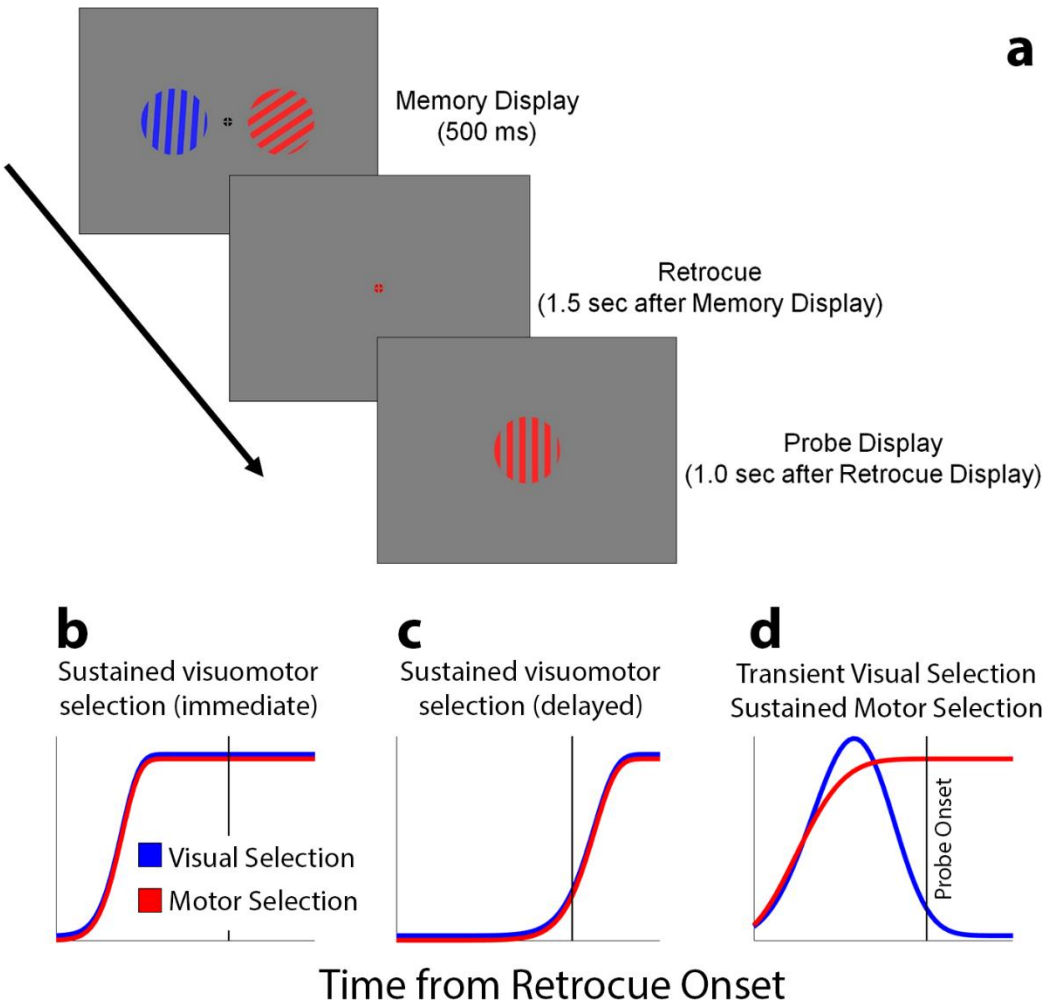

Fig. 1. Retrospectively Cued Visuomotor Selection Task and Possible Outcomes. *(a) Retrospectively cued orientation recall task. See text and Supporting Online Materials for more details. visual and motor selection. (b-d) Hypothetical time courses of visual and motor selection.*

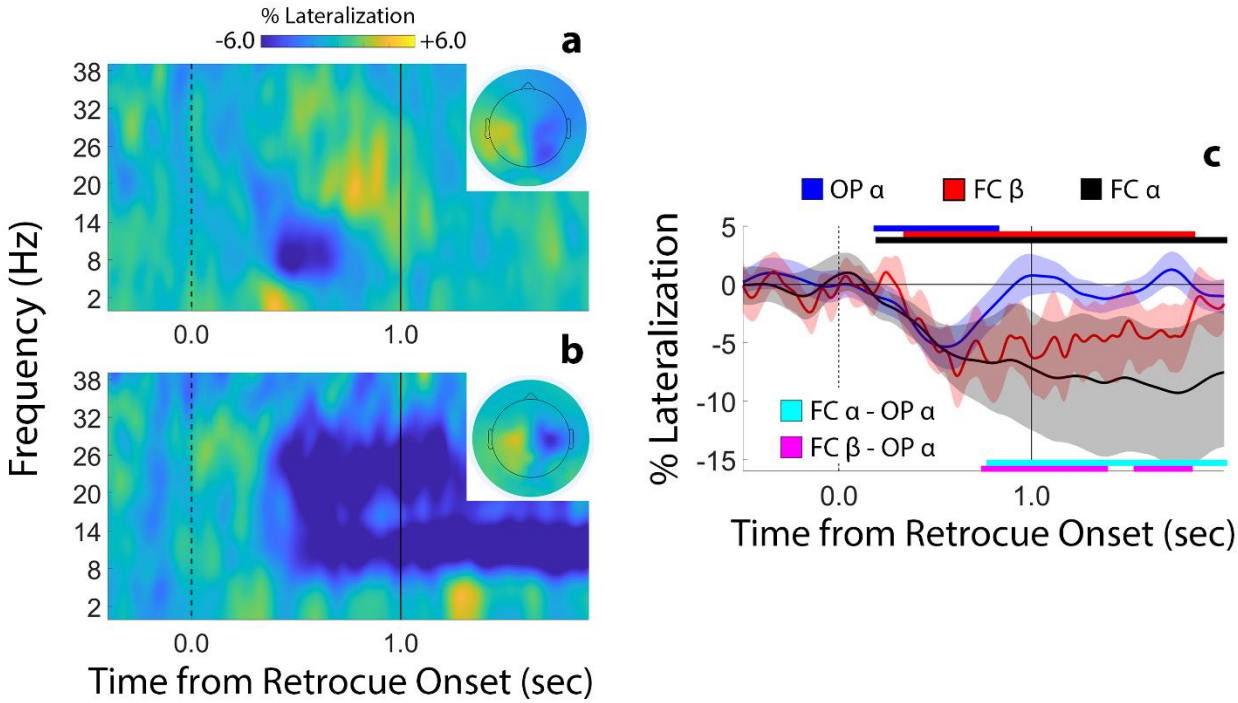

Fig. 2. Spectral signals associated with visual and motor selection during WM-guided behavior. *(a) Broadband frequency-specific lateralization over 10-20 occipitoparietal electrode site pairs O1/2, PO3/4, and PO7/8. Inset shows the distribution alpha-power lateralization (8-13 Hz) over all recorded electrode sites. (b) Broadband frequency-specific lateralization over 10-20 frontocentral electrode site pairs C1/2 and C3/4. Inset shows the distribution of beta-power lateralization (15-30 Hz) over all recorded electrode sites. (c) Occipitoparietal alpha-power lateralization, frontocentral alpha-power lateralization, and frontocentral beta-power lateralization time-locked to retrocue onset. Blue, red, and black bars at the top of the plot show periods where occipitoparietal/frontocentral lateralization was < 0. Cyan and maroon bars at the bottom of the plot show periods where frontocentral alpha lateralization was significantly greater than occipitoparietal alpha lateralization and periods where frontocentral beta lateralization was significantly different from occipitoparietal alpha lateralization, respectively. Shaded regions depict the 95% confidence interval of the mean. The vertical lines at time 0.0 and 1.0 depict the onset of the retrocue and probe displays, respectively. OP = occipitoparietal, FC = frontocentral.*

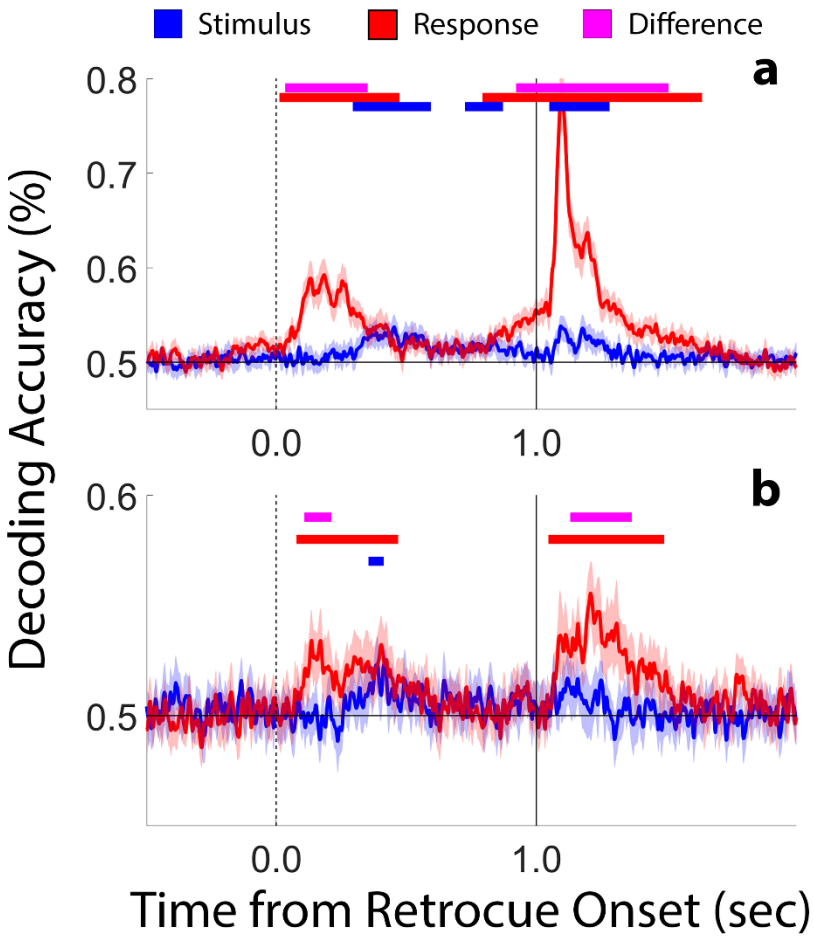

Fig 3. Location and Response Hand Decoding Performance in Occipitoparietal (a) and Frontocentral (b) Electrode Clusters. *We used a linear discriminant classifier (see Supporting Online Methods) to predict the location of the retrospectively cued grating (i.e., left vs. right visual field) and response hand (i.e., left vs. right hand) from broadband activity measured at occipitoparietal electrode clusters (O1/2, PO3/4, PO7/8; panel a) and frontocentral electrode clusters (C1/2, C3/4; panel b). Note that stimulus location and response hand were randomly and independently manipulated across trials; thus, similarities and/or differences in decoding performance across electrode clusters cannot be explained by volume conduction or signal mixing. Decoding time courses have been smoothed with a 10 ms Gaussian kernel for presentation; smoothing had no qualitative effect on statistical conclusions. Shaded regions around each line depict the 95% confidence interval of the mean. Blue and red bars at the top of each plot depict epochs where stimulus location and response hand decoding were significantly greater than chance (50%; nonparametric cluster-based permutation test; see Supporting Online Methods); maroon lines depict intervals where response hand decoding was significantly greater than stimulus location decoding. Vertical lines at time 0.0 and 1.0 depict the onset of the retrocue and probe displays, respectively.*